Hydrodynamics of back spatter by blunt bullet gunshot with a link to bloodstain pattern analysis

P. M. Comiskey,[1] A. L. Yarin,[1,*] and D. Attinger[2]
[1]*Department of Mechanical and Industrial Engineering, University of Illinois at Chicago, 842 West Taylor Street, Chicago, Illinois 60607-7022, USA*
[2]*Department of Mechanical Engineering, Iowa State University, 2529 Union Drive, Ames, Iowa 60011-1210, USA*
(Received 30 March 2017; published 24 July 2017)

A theoretical model describing the blood spatter pattern resulting from a blunt bullet gunshot is proposed. The predictions are compared to experimental data acquired in the present work. This hydrodynamic problem belongs to the class of the impact hydrodynamics with the pressure impulse generating the blood flow. At the free surface, the latter is directed outwards and accelerated toward the surrounding air. As a result, the Rayleigh-Taylor instability of the flow of blood occurs, which is responsible for the formation of blood drops of different sizes and initial velocities. Thus, the initial diameter, velocity, and acceleration of the atomized blood drops can be determined. Then, the equations of motion are solved, describing drop trajectories in air accounting for gravity, and air drag. Also considered are the drop-drop interactions through air, which diminish air drag on the subsequent drops. Accordingly, deposition of two-phase (blood-drop and air) jets on a vertical cardstock sheet located between the shooter and the target (and perforated by the bullet) is predicted and compared with experimental data. The experimental data were acquired with a porous polyurethane foam sheet target impregnated with swine blood, and the blood drops were collected on a vertical cardstock sheet which was perforated by the blunt bullet. The highly porous target possesses a low hydraulic resistance and therefore resembles a pool of blood shot by a blunt bullet normally to its free surface. The back spatter pattern was predicted numerically and compared to the experimental data for the number of drops, their area, the total stain area, and the final impact angle as functions of radial location from the bullet hole in the cardstock sheet (the collection screen). Comparisons of the predicted results with the experimental data revealed satisfactory agreement. The predictions also allow one to find the impact Weber number on the collection screen, which is necessary to predict stain shapes and sizes.

DOI: 10.1103/PhysRevFluids.2.073906

I. INTRODUCTION

Bloodstain pattern analysis (BPA) is the physical inspection of bloodstain patterns [1] to provide a criminal (or accident-related) investigation with answers to the following questions: (i) What physical mechanisms could have caused the patterns? (ii) What were the positions (or trajectories) of the persons and objects involved? (iii) When were the bloodstains produced? A blood spatter pattern is a collection of bloodstains located on a solid surface produced by airborne drops [1], typically occurring in blunt-force (beating) or gunshot cases. In relation to question (ii), blood spatters have been interrogated to determine the relative position of the alleged criminals with respect to their victims. However, BPA techniques available to crime scene investigators to reconstruct droplet trajectories currently are not based on the latest knowledge of fluid dynamics [2]. For instance, some BPA techniques neglect the contributions of air drag and gravity [2]. Those currently used techniques, called the method of strings or the trigonometric method, assume that drops travel in straight lines.

*Corresponding author: ayarin@uic.edu

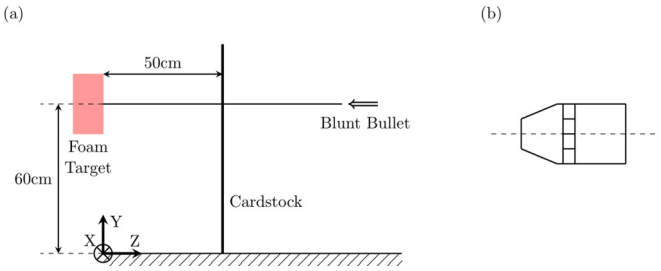

FIG. 1. (a) Schematic of experimental setup with the cardstock used for back spatter collection. The X axis is directed from the reader and the coordinate trihedron is located on the floor under the center of the target shot by the bullet. (b) Bullet shape.

In some situations, this assumption gives rise to large uncertainties [2,3] in the determination of the region of origin of a blood spatter, and of the relative positions of the persons involved, as in the famous trials of music producer Spector and physician Shepard [2]. Also, a sound physical theory describing the fluid mechanics of the blood pattern formation is not yet available to BPA practitioners [4]. Thus, a lot of the quantitative information from the crime scene such as the number of stains, their spatial distribution, and their area are left out of current crime scene reconstruction. This information should not be neglected because it could help to differentiate between spatter types, for example, blood patterns produced in forward spatter and backward, or blunt-force versus shooting spatters [5]. It is therefore imperative to develop hydrodynamic models of blood spatter [2], as for example [4] where the formation of blood drops was attributed to the Rayleigh-Taylor instability. That instability necessarily occurs when denser blood is accelerated towards lighter air [6], which is the case when blood deforms following a bullet impact.

Once a cloud of blood drops is generated due to a gunshot, its behavior in a sense is reminiscent of that of a sprinkler or diesel-engine jets studied previously in [7,8]. Such jets entrain significant volumes of air. The resulting two-phase flow diminishes the aerodynamic drag of drops moving behind the leading ones, similarly to the V formation of a flying flock of birds [9]. Then, the prediction of drop trajectories in such jets makes use of the initial drop sizes and initial velocities resulting from the Rayleigh-Taylor instability and proceeds, accounting for gravity and air drag forces, with the latter being diminished by the drop-drop interaction through air mentioned above [7]. It should be emphasized that few other studies account for gravity and air drag (albeit without accounting for the drop-drop interaction) to predict blood spatter patterns [10–12], however, they do not consider the physical mechanism of drop formation.

The recent theory of the back spatter of blood was developed specifically for slender bullets [4], e.g., full metal jacket bullets. Here we propose the fluid mechanical theory of blood back spatter from blunt bullets. This theory is compared with the experiments also conducted in this work. The experiments are described in Sec. II, the theory is presented in Sec. III, results are discussed in Sec. IV, and conclusions are drawn in Sec. V.

II. EXPERIMENT

Experiments with back spatter resulting from a blunt bullet impact were performed at the indoor shooting range in Izaak Walton League Park in Ames, Iowa, USA. The experimental conditions are presented in Fig. 1 and summarized in Table I.

A cardstock sheet ($141.4 \times 111.4\,\mathrm{cm}^2$) was used to collect the backward spattered drops and was located vertically between the muzzle of the gun and the target (see Fig. 1). The bullet trajectory was parallel to the ground at a height of 60 cm and after penetrating through the cardstock sheet traveled 50 cm until the impact with the target, at which point blood spattered backward toward the collecting sheet. A high-density fiberboard pierced with a hole twice the diameter of that bullet's

TABLE I. Experimental parameters.

Condition	Type and specifications
Rifle	Rock River Arms, LAR-15 16" barrel M-4, .223 cal with Yanki YHM Phantom 223 suppressor.
Bullet	Hollow point BEE .224 cal (corresponding to a diameter of 5.7 mm, 45 grain).
Casing and explosive loading	.223 Remington: powder: BLC-2 powder weight: 26.5 grains primer: Winchester Small Rifle Primer case: once fired Federal & Winchester.
Target	Polyurethane foam sheet ($16 \times 23 \times 10.5\,\mathrm{cm}^3$), wrapped around a cardboard piece and held with binder clips.
Fluid	Swine blood with ACD anticoagulant, hematocrit of 41%, drawn two days before the experiment, blood heated to $37 \pm 2\,^{\circ}\mathrm{C}$ before being clipped in target position.
Room	$44 \pm 5\%$ relative humidity $16.8 \pm 1\,^{\circ}\mathrm{C}$ room temperature

was placed between the gun and the cardstock, to minimize the interference of the muzzle gases (a topic of future research) with the back spatter process, which can either modify the drop trajectories, or dynamically deform the cardstock. Two experiments were performed under the same conditions. Then the collecting sheet was removed and digitized with a 600-DPI scanner. The information on stain location, number of drops, and area (which was acquired via pixel density), were all found with a purpose-developed in-house program. The in-house program lumped the stain characteristics into a set of bins corresponding to 11 concentric disk-shaped areas with the following upper radial bounds in centimeters: 2, 4, 6, 9, 12, 18, 24, 30, 40, 60, and 90.

III. THEORY

A. Blood flow induced by a blunt bullet impact

The blunt (hollow point) bullet shown in Fig. 1(b) has a front edge which resembles a disk. The impact duration $\tau \sim 1\,\mu$s, and the impact velocity $V_0 \approx 1000\,\mathrm{m/s}$, is at least of the order of the speed of sound in blood and is supersonic relative to air. Then, the impact pressure $\Delta p \sim \rho V_0 C_s$ where C_s is the speed of sound in blood and ρ is its density. Essentially, this is the situation where $\Delta p \to \infty$, $\tau \to 0$, and the impulse $\Pi = \int_0^\tau \Delta p dt = O(1)$, with t being time. Such situations are characteristic of impact-driven fluid mechanics, where the flows are inevitably potential, with the potential $\varphi = -\Pi/\rho$ [13–16]. Accordingly, the flow potential satisfies the axisymmetric Laplace equation

$$\nabla^2 \varphi = \frac{1}{r}\frac{\partial}{\partial r}\left(r\frac{\partial \varphi}{\partial r}\right) + \frac{\partial^2 \varphi}{\partial z^2} = 0, \tag{1}$$

with r and z being the radial and axial coordinates, respectively. The z coordinate is reckoned along the axis of symmetry of the bullet, is zero at the free surface, and is positive in the direction away from the free surface into the liquid bulk.

The potential solution of Eq. (1) is finite at the z axis in the liquid bulk

$$r = 0 : \varphi < \infty. \tag{2}$$

At the free surface the boundary conditions read

$$z = 0 : \frac{\partial \varphi}{\partial z} = V_0 \quad \text{at} \quad 0 < r < a, \tag{3}$$

$$z = 0 : \ \varphi = 0 \quad \text{at} \quad a < r < \infty, \tag{4}$$

where a is the radius of the blunt bullet edge.

In the far field within the liquid bulk the no-flow boundary condition is imposed,

$$z = \infty : \ \frac{\partial \varphi}{\partial z} = 0. \tag{5}$$

The problem (1)–(5) is singular because of the boundary conditions (2) and (4) (the axis of the cylindrical coordinate system, and the radially infinite domain, respectively). Accordingly, being solved using variable separation, it possesses a continuous spectrum ν, with the result being expressed in the form of the following Fourier-Bessel integral:

$$\varphi = \int_0^\infty D_\nu J_0(\nu r) e^{-\nu z} d\nu, \tag{6}$$

where D_ν is a constant, i.e., it does not depend on either r or z.

Accordingly, the z component of flow velocity at the moment of impact is

$$v_z = \frac{\partial \varphi}{\partial z} = -\int_0^\infty D_\nu \nu J_0(\nu r) e^{-\nu z} d\nu. \tag{7}$$

Accordingly, the boundary conditions (3) and (4) with the help of Eqs. (6) and (7) take the following form:

$$-\int_0^\infty D_\nu \nu J_0(\nu r) d\nu = V_0 \quad \text{for } 0 < r < a, \tag{8}$$

$$-\int_0^\infty D_\nu J_0(\nu r) d\nu = 0 \quad \text{for } a < r < \infty. \tag{9}$$

Introducing $\xi = r/a$ and $\eta = \nu a$, Eqs. (8) and (9) are transformed to the following form:

$$\int_0^\infty D_\nu \eta J_0(\eta \xi) d\eta = -V_0 a^2 \quad \text{for } 0 < \xi < 1, \tag{10}$$

$$\int_0^\infty D_\nu J_0(\eta \xi) d\eta = 0 \quad \text{for } 1 < \xi < \infty. \tag{11}$$

It is easy to check that Eqs. (10) and (11) are satisfied with

$$D_\nu = \frac{2}{\pi} V_0 a^2 \left(\frac{\cos \eta}{\eta} - \frac{\sin \eta}{\eta^2} \right). \tag{12}$$

Substituting Eq. (12) into Eq. (6), we arrive at the following expression for the flow potential at the blunt bullet edge

$$\varphi|_{z=0} = \frac{2}{\pi} V_0 a \int_0^\infty \left(\frac{\cos \eta}{\eta} - \frac{\sin \eta}{\eta^2} \right) J_0(\eta \xi) d\eta \quad \text{for } 0 < \xi < 1. \tag{13}$$

The integrals in Eq. (13) can be evaluated, which yields

$$\varphi|_{z=0} = -\frac{2}{\pi} V_0 \sqrt{a^2 - r^2} \quad \text{for } 0 < r < a. \tag{14}$$

Also, Eqs. (6) and (12) yield the radial and axial velocity components at the free surface $1 < \xi < \infty$,

$$v_r|_{z=0} = \frac{\partial \varphi}{\partial r} = -\frac{2}{\pi} V_0 \int_0^\infty \left(\cos\eta - \frac{\sin\eta}{\eta}\right) J_1(\eta\xi) d\eta, \tag{15}$$

$$v_z|_{z=0} = \frac{\partial \varphi}{\partial z} = -\frac{2}{\pi} V_0 \int_0^\infty \left(\cos\eta - \frac{\sin\eta}{\eta}\right) J_0(\eta\xi) d\eta. \tag{16}$$

Evaluating the integrals in Eqs. (15) and (16), one obtains

$$v_r|_{z=0} = 0 \quad \text{for } a < r < \infty, \tag{17}$$

$$v_z|_{z=0} = -\frac{2}{\pi} V_0 \left[\frac{a}{\sqrt{r^2 - a^2}} - \arcsin\left(\frac{a}{r}\right)\right] \quad \text{for } a < r < \infty. \tag{18}$$

The latter equation can be found in [15]. Note also that $v_z|_{z=0} < 0$, i.e., the flow at the free surface is directed outward, toward air. The impulsive motions are established on the time scale $\tau = ca/V_0$ where c is a dimensionless factor. Accordingly, the acceleration of blood at the free liquid surface, A, can be evaluated using Eq. (18) as

$$A(r) \approx -\frac{2}{\pi} \frac{V_0^2}{ca} \left[\frac{a}{\sqrt{r^2 - a^2}} - \arcsin\left(\frac{a}{r}\right)\right]. \tag{19}$$

The impact velocity that generates the impulsive motions V_0 is less than the bullet approach velocity V_a, because the propagation of the sound wave within the liquid absorbs a part of the kinetic energy of the bullet. Accordingly [16–18],

$$V_0 = V_a \frac{1}{1 + 4\rho a^3/(3m)}, \tag{20}$$

where m is the bullet mass. For the bullet used in the experiments, the approach velocity is $V_a \approx 1000\,\text{m/s}$, while $a = 0.285\,\text{cm}$, and $m = 2.916\,\text{g}$, which results in $V_0 = 988.90\,\text{m/s}$.

B. Blood droplet size distribution and ejection due to the Rayleigh-Taylor instability

The surface of splashed blood accelerated toward air is subjected to the Rayleigh-Taylor instability [7]. The fastest growing wavelength of such instability defines the characteristic drop size l_*, which is understood as its diameter,

$$l_*(r) = \frac{2\pi}{\sqrt{\rho |A(r)|/(3\sigma)}} w, \tag{21}$$

where σ is the surface tension of blood and w is a dimensionless factor. The factor w appears due to the fact that Eq. (21) is an order of magnitude estimate. Due to the action of surface tension, the launched blood droplets maintain a spherical shape and are assumed to carry that shape until impact. Note that as $r \to \infty$, the acceleration tends to zero, and thus, $l_* \to \infty$. A practically relevant cutoff used in this work was $r_{\max} = 5a$.

Equations (18) and (21) show that smaller, faster drops originate close to the impacting blunt bullet while the larger and slower ones are formed further from it.

The continuous drop population can be dissected into subfamilies with masses M_i as

$$M_i = \rho\tau \int_{b_i}^{b_{i+1}} |v_z|_{z=0}| 2\pi r dr, \tag{22}$$

where the limits correspond to a subfamily i, $b_i \leqslant r \leqslant b_{i+1}$. The integral of Eq. (22) can be evaluated with Eq. (18) resulting in

$$M_i = 4\rho c a \left\{ a\left[\sqrt{b_{i+1}^2 - a^2} - \sqrt{b_i^2 - a^2}\right] - \frac{1}{2}\left[b_{i+1}^2 \arcsin\left(\frac{a}{b_{i+1}}\right) - b_i^2 \arcsin\left(\frac{a}{b_i}\right) + a\sqrt{b_{i+1}^2 - a^2} - a\sqrt{b_i^2 - a^2}\right]\right\}. \tag{23}$$

The dimensionless factor c corresponds to the fact that an order of magnitude of the impact time τ is used.

The number of droplets in each subfamily can then be found as

$$n_i = \frac{M_i}{\rho\pi l_{*,i}^3/6}. \tag{24}$$

C. Blood droplet spray propagation

Calculation of the drop trajectories, using the coordinate frame defined in Fig. 1, is described in detail in our previous work [4], and is briefly outlined here.

The continuous spectrum of droplets issued as a result of the Rayleigh-Taylor instability was dissected into discrete groups (bins, denoted by numerals i). These bins were considered as interpenetrating continua with air which was entrained into motion by viscous suction due to the eddy viscosity. Individual blood droplets from bin i experience air drag expressed using the drag coefficient correlation already used for the forensic applications in [2,4], namely,

$$C_{D,i} = 0.28 + \frac{6}{\mathrm{Re}_i^{0.5}} + \frac{21}{\mathrm{Re}_i} \quad \text{for the Reynolds number } 0.1 \leqslant \mathrm{Re}_i \leqslant 4000. \tag{25}$$

In a dense spray, like those in blood spatter, air entrainment is dominated by the fastest moving droplets "leading" the spray (the two-phase jet), whereas the other droplets are moving in the aerodynamic wake of the leading ones and experience either no aerodynamic drag, or a significantly diminished drag, as was previously shown for sprinkler jets and diesel sprays [7,8] and implemented in the predictions of backward spatter in [4]. The effect of the aerodynamic wake of the preceding droplets can be so severe that the trailing droplets can be even accelerated due to it, as it was recently shown in the analysis of high-speed video observations of backward spatter caused by gunshots [19].

In distinction from [4], only a normal impact of a bullet onto the target is considered, i.e., the impact inclination angle $\delta = 0^\circ$. Also, it is assumed that the radius of the impact of the disklike area of a blunt bullet is much smaller than the distances travelled by the spatter drops. As in [4], a set of discrete angular positions of the disk where drops are spattered is considered, which corresponds to a set of discrete values of the polar angle Φ in the disk plane. The angular positions on the disk begin from $\Phi = 0$, which is the rightmost point of the disk, and increase with $\Delta\Phi = \pi/12$. Then, $\Phi = \pi/2$ corresponds to the topmost point of the disk, $\Phi = \pi$ corresponds to the leftmost point, etc. Then, according to [4], the initial angle of inclination of drop trajectories, ψ, is given by

$$\psi = \arcsin\left[\sin(\Delta\theta)\sin(\Phi)\right], \tag{26}$$

where $\Delta\theta$ is the angle of the spatter relative to the bullet axis. This angle is discussed in more detail in Sec. IV.

The distances reached by drops in their plane of flight are denoted as Z_φ and, as in [4], they correspond to the normal distance from the target Z given by the following expression:

$$Z = Z_\varphi \frac{\cos(\Delta\theta)}{\sqrt{\cos^2(\Delta\theta) + \sin^2(\Delta\theta)\cos^2(\Phi)}}. \tag{27}$$

In the direction parallel to the target surface these droplets are deposited at points with the lateral coordinate X given by

$$X = Z[\tan(\Delta\theta)\cos(\Phi)]. \tag{28}$$

In the case of drop deposition on a vertical sampling cardstock located at a known distance from the target, the latter determines the value of Z_φ entering Eq. (27) (and thus Z), the lateral coordinate of the stain is given by Eq. (28), and its final height on the cardstock is directly found from the governing trajectory equations of [4].

IV. RESULTS AND DISCUSSION

The scanned images of the cardstock sheet, which was located vertically at a distance of 50 cm from the target and perforated by a blunt bullet, were discretized radially from the penetration location to the furthest drop into ten concentric disk-shaped areas of equal width. In each ring-shaped segment, the number of stains was counted and summed to find the number of stains per segment. Also, the average stain area and the total stain area per segment were found. These values were attributed at the location of the mid radius of each segment. This procedure resulted in ten data points for the number of drops, the average stain area, and the total stain area as the functions of the radial coordinate from the blunt bullet penetration location on the vertical collector sheet.

It should be emphasized that the theory of Sec. III attributes formation of blood drops in back spatter to the very first moment of the impact of the blunt edge of the bullet onto the target. Therefore, the theoretical predictions are unaffected by the following disintegration of the bullet, which happens in the experiments. To compare the theoretical data with the results of the experiment described in Sec. II, several parameters must first be defined. The following values were used in the simulations: the blunt bullet impact velocity $V_0 = 988.90$ m/s (corresponding to a bullet approach velocity of $V_a \approx 1000$ m/s), radius of the impact area of the blunt bullet (a disk), $a = 0.285$ cm, the spatter spread angle, $\Delta\theta = 15^\circ$, the azimuthal discretization in the angular direction, $\Delta\Phi = \pi/12$, the height of the impact, $H_0 = 56.0$ cm, and the dimensionless factors were $w = 0.112$ and $c = 786.6$ (for a blunt bullet). In comparison, the latter two factors in [4] were taken as $w = 0.9$ and $c = 0.001$ (for a slender bullet). The drop size generated by a gunshot via the Rayleigh-Taylor instability should be definitely affected by the bullet shape, which explains variation in the value of w [in the same order of magnitude in Eq. (21)]. Also, it should be emphasized that the amount of blood splashed by a blunt bullet is usually larger than that of a slender bullet. That is reflected by a different, much larger, value of c used in the present work. Ultimately, the value of c is affected by the bullet shape, as one of the factors, and the increased value used here reflects that fact.

The chosen value of $\Delta\theta = 15^\circ$ can be substantiated on the basis of several published experiments and on our theoretical analysis. The x-ray measurements during impact of metallic projectiles in water in [20] revealed a conical cavity trailing the projectile with $10^\circ < \Delta\theta < 20^\circ$, for diameters and supersonic (by air) impact velocities comparable to that of our study. Interestingly, [20] reported similar values of $\Delta\theta$ for projectiles with various shapes, such as spheres, cylinders, with spherical tips, and blunt cylinders. Similar values of $10^\circ < \Delta\theta < 20^\circ$ were reported in [21] for impacts of spheres in water at both low and high Bond numbers. The authors of [22,23] used shadowgraphy to estimate the pressure field in the fluid around the projectile.

A theoretical justification of the value of $\Delta\theta$ in the present case of a blunt bullet atomization of blood can be made as follows. According to Eq. (17) the radial velocity of splashed liquid is equal to zero, and thus the initial ejection is expected to be strictly normal to the free surface. This is indeed observed in the intact crownlike splashes resulting from drop impact onto a liquid surface (cf. Fig. 6 in [24]). However, in the present case the ejected liquid is atomized practically from the very beginning, which results in the suction of a significant mass of air, which inevitably happens at the periphery of the spattered two-phase blob unaffected by any aerodynamic effects caused by a bullet (cf. Fig. 4 in [19]). Accordingly, the ejected drop blob essentially forms an axisymmetric two-phase submerged turbulent jet. This fact is accounted for in the present model following our previous work [4] in the

calculation of the air mass entrained by the moving drop-air blob. It should be emphasized that due to the air entrainment the drop-air blob widens to compensate for the decrease of its velocity due to the action of the eddy viscosity and sustains the invariant value of the longitudinal momentum flux [25]. Accordingly, the asymptotic boundary of the two-phase jet associated with the one-tenth longitudinal velocity u in comparison to the corresponding axial velocity value u_m is given by $y_{0.1} = \eta_{0.1} a_T x$, where $\eta_{0.1}$ is the value of the self-similar coordinate corresponding to the boundary and a_T is the semiempirical constant of the Prandtl mixing length theory ($a_T = 0.045 - 0.055$) [25]. Since the self-similar velocity profile in the jet cross-section is given by $u/u_m = (1 + \eta^2/8)^{-2}$, the value of $\eta_{0.1}$ is found as $\eta_{0.1} = [8(\sqrt{10} - 1)]^{1/2} = 4.16$. Then, $\tan \Delta\theta = dy_{0.1}/dx = \eta_{0.1} a_T = 0.229$ (with the value $a_T = 0.055$ being used). Accordingly, $\Delta\theta = 13^\circ$, which is close to the value of $\Delta\theta = 15^\circ$ used in the calculations.

Note that in [16,21] theoretical models for the evolution of the splash curtain formed at high Weber number are presented, still in the velocity range well below that of a gunshot. Also, the work [26] explains theoretically that the cavity shape is identical for various projectile shapes, provided that the ratio of their cross-section times drag coefficient over their mass would be the same, which was verified in [27].

Note also that the case of a backspatter caused by a conical bullet [4] belongs to the class of the entry (Wagner) problems where a wedgelike or an axisymmetric body penetration into liquid is accompanied by a splashed liquid jet rising over the body generatrix and forming a thin sheet prone to atomization. The entry problems, which are essentially different from the instantaneous impact problem we are dealing with here, were studied in detail in the following works and references therein [15–18,28–30]. Recently, it was shown experimentally that the splashed liquid jet rising over the body generatrix as a consequence of the body entry is displaced from the body surface due to the air gulping, which can further affect the liquid atomization process in such situations [31]. In typical BPA cases, muzzle gases can also deflect the ejected blood drops, as the experimental data discussed in [19] revealed. In particular, the effect of the muzzle gases and the underlying bones could cause $\Delta\theta \approx 90^\circ$, as in [32]. In the present study however, the influence of the muzzle gases has been made negligible by design of the experimental setup.

The experimental data in Fig. 2 reveal a significant difference in the total number of droplets between the two sets of experimental data. The reasons for the differences are not clear to us at the present time. The experimental trends, however, are similar, and the theoretical predictions closely follow the data of the experiment T13. The results reveal a steep rise in the number of drops which peak for a characteristic maximum around a distance of about 15–20 cm from the location where the cardstock was penetrated by the bullet followed by a gradual decrease in the number of drops deposited further on.

It is important to note that the experiments in Fig. 2 show a maximum spatial concentration of stains at ~20 cm from the bullet hole. Considering the distance of 50 cm between the substrate and the cardstock sheet, this corresponds to a spatter spread angle $\Delta\theta = \tan^{-1}(20/50) = 21^\circ$, close to $\Delta\theta = 15^\circ$, the value used in the calculations.

In a normal drop impact the stain is larger than the original drop size by the spread factor ξ [33–35],

$$\xi = 0.61 \left(\frac{\mathrm{We}_f}{\mathrm{Oh}_f} \right)^{0.166}, \tag{29}$$

where We_f and Oh_f are the final (impact) Weber and Ohnesorge numbers, respectively,

$$\mathrm{We}_f = \frac{\rho l_{*i} u_{i,f}^2}{\sigma}, \quad \mathrm{Oh}_f = \frac{\sqrt{\mathrm{We}_f}}{\mathrm{Re}_{i,f}} \tag{30}$$

(note that the latter expressions involve two physical parameters of blood: its density $\rho = 1.06\,\mathrm{g/cm^3}$, and its surface tension $\sigma = 60.45\,\mathrm{g/s^2}$ [36]). The subscript i in Eqs. (30) indicates each drop subfamily (cluster) in the simulations, f stands for final, and $\mathrm{Re}_{i,f}$ is the final Reynolds number for

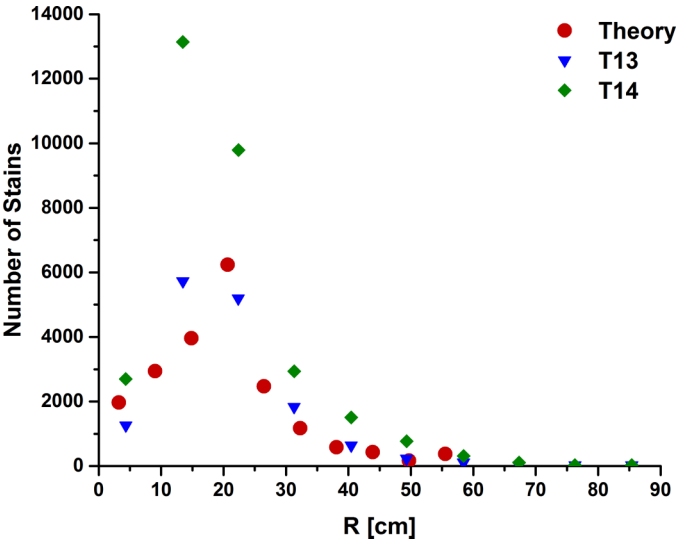

FIG. 2. Predicted and measured number of drops in back spatter at different radial locations relative to the bullet path at a vertical cardstock collector at 50 cm before the target. Red circles show the theoretical prediction, blue triangles show the data of experiment T13, and green diamonds show the data of experiment T14.

each cluster. Since in the present case of back spatter drop impact on a vertical cardstock sheet the impacts are not normal and therefore the spread factor alone cannot account for the arising stain area, a relation with the impact angle must be found. Using the approach employed for crime scene reconstruction [37], the relation between the longest size of drop stain, L, resulting from an oblique impact, and the stain size after normal impact, $\xi \ell_*$ [cf. Eqs. (21) and (28)] can be taken as

$$L = \xi \frac{l_*}{\sin \alpha} \tag{31}$$

with the angle α shown in Fig. 3. Accordingly, the effective stain area is evaluated as

$$A = \frac{\pi l_*^2 \xi^2}{4 \sin \alpha}. \tag{32}$$

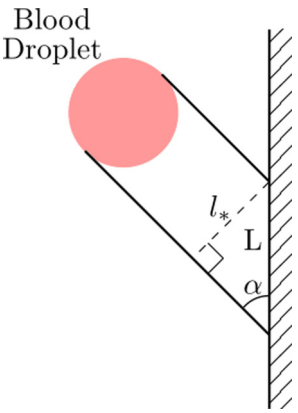

FIG. 3. Stain formation in oblique drop impact onto a vertical surface.

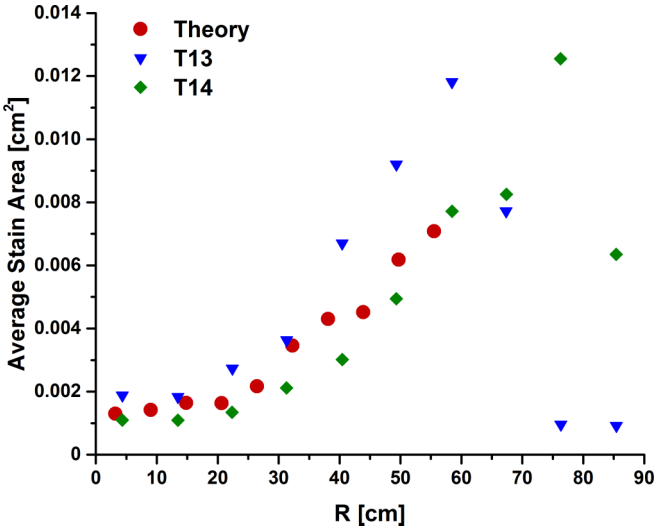

FIG. 4. Comparison of the predicted and measured average stain area on the vertical collector located at 50 cm before the target. Red circles depict the theoretical prediction, blue triangles correspond to the experiment T13, and green diamonds to the experiment T14.

The predicted average stain area on the vertical collector located at 50 cm before the target is compared in Fig. 4 to the measured one and the agreement is quite satisfactory. The values of l_* in Eq. (32) calculated using Eq. (21) for five clusters are shown in Table II. It should be emphasized that the pore size in the target sponge is of the order 0.1 cm, i.e., is an order of magnitude larger than the drop size l_* determined by the Rayleigh-Taylor instability (cf. Table II). This means that the pores hardly impose a significant hydraulic resistance. Nevertheless, due to a relatively high surface tension of blood ($\sigma = 60.45\,\mathrm{g/s^2}$), individual blood jets issued from the pores will immediately merge and form an intact layer, as observed in the experiments with high surface tension liquids in [38]. In distinction from [38], this intact liquid layer is subjected to tremendously high acceleration toward air and thus is prone to the Rayleigh-Taylor instability which sets an ultimate drop size. Note also that when a target sponge is covered by tape or silicone (not the case in the present work), the blood spatter can be affected causing an uneven distribution of drops [19].

Figure 4 reveals that, on average, in back spatter, smaller drops land on the vertical collector closer to the penetration location of the blunt bullet than the larger ones. It should be emphasized that the largest drops land at the furthest locations. The number of drops times their average stain area at a certain location yield the total stain area for their respective radial locations, which is illustrated in Fig. 5.

TABLE II. Characteristic drop cluster sizes calculated using Eq. (21).

Cluster	l_* (mm)
1	0.1932
2	0.2242
3	0.2566
4	0.2903
5	0.3254

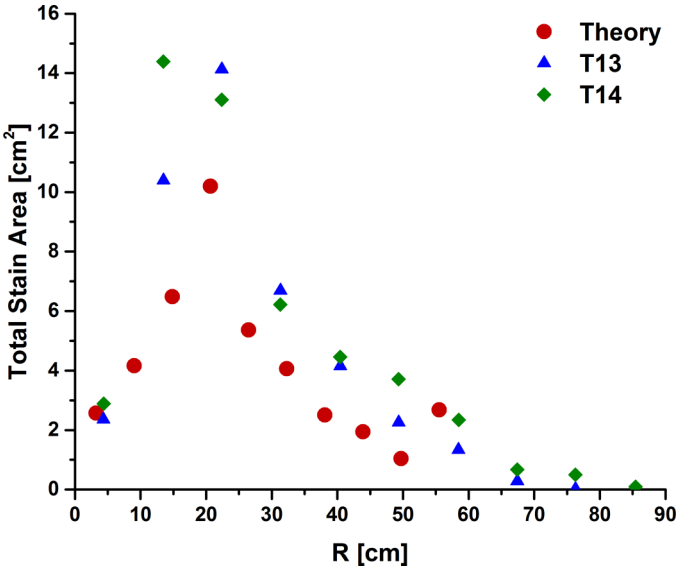

FIG. 5. Comparison of the predicted and measured total stain area on the vertical collector located at 50 cm before the target. Red circles depict the theoretical predictions, blue triangles correspond to the experiment T13, and green diamonds to the experiment T14.

The experimental data sets fall on top of one another in Fig. 5 because T13 has a lower total number of droplets yet a larger average stain area, and vice versa for T14. It is interesting to note the plateau in the $R = 35 - 50$-cm range. This plateau is also seen in the theoretical predictions, albeit to a lesser extent. The numerical predictions also allow one to find the final impact angle and the

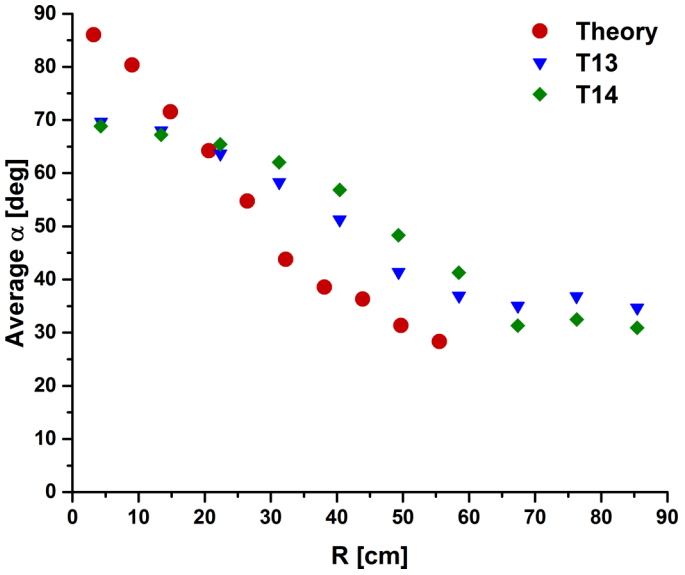

FIG. 6. Predicted impact angle lumped over consecutive rings on the vertical collector screen located at 50 cm before the target. The angle is reckoned from the vertical collector screen direction. Red circles depict the theoretical predictions, blue triangles correspond to experiment T13, and green diamonds to the experiment T14. Note that the main discrepancy between theoretical and experimental data is for results close to the bullet hole.

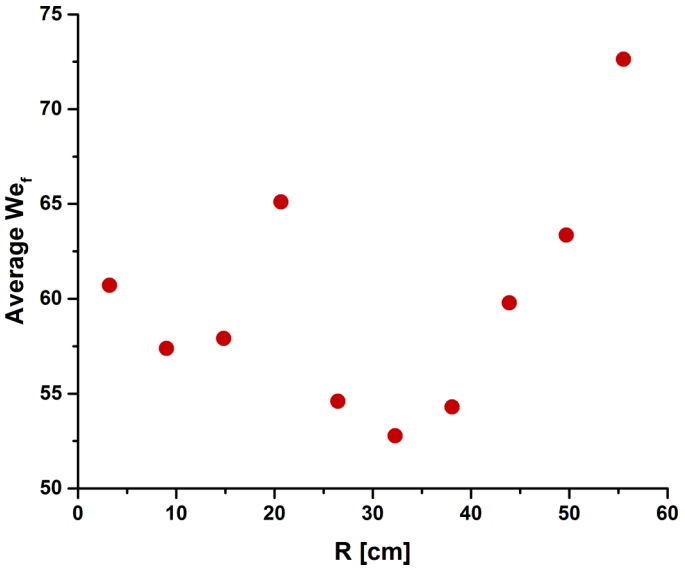

FIG. 7. Dependence of the average final Weber number as a function of the radial coordinate predicted numerically.

impact Weber number on the collection screen. This can be done with the same radial discretization as in Figs. 2, 4, and 5.

The impact angle α relative to the vertical collector screen depicted in Figs. 6 reveal that the larger drop impacts such a collector more tangentially than the smaller ones and at a further radial distance from the bullet path. Note that the main discrepancy between theoretical and experimental data is for the locations close to the bullet hole. This may be due to the experimental data collection process where tears of cardstock at the periphery of the bullet hole are interpreted as stains. The final Weber number, averaged over each ring-shaped segment, is shown in Fig. 7.

V. CONCLUSION

A theoretical model is proposed for predicting bloodstain patterns from back spatter resulting from a blunt bullet. The model attributes the back spatter to the Rayleigh-Taylor instability of the free surface of blood, and thus extends the previously proposed model for the back spatter due to slender bullets. The drop flight through air from the target to the deposition surface (in the present case a vertical sheet of cardstock located between the shooter and the target) is predicted accounting for gravity and air drag. The latter incorporated the collective effect associated with the drag reduction on the drops following the previous drops in their aerodynamic wake. The predicted and measured number of drops, the average stain area, and the total stain area as functions of the radial distance from the penetration point on the deposition surface are found to be in a fairly good agreement. Future work will consider the additional complexity of the interaction of the muzzle gases with the atomization and spattering processes, and also assess the practical implications of these experiments and theoretical predictions for the criminal justice system.

ACKNOWLEDGMENTS

The authors acknowledge financial support from the US National Institute of Justice (Grant No. NIJ 2014-DN,BX,K036). This work was partially funded by the Center for Statistics and Applications in Forensic Evidence (CSAFE) through Cooperative Agreement No. 70NANB15H176 between

NIST and Iowa State University, which includes activities carried out at Carnegie Mellon University, University of California Irvine, and University of Virginia. The authors gratefully recognize the help of D. R. Van Ryswyk. Technical assistance of S. Kim and J. Polansky in the hematocrit measurement and acquisition of the blood spatters is gratefully acknowledged.

---

[1] T. Bevel and R. M. Gardner, *Bloodstain Pattern Analysis with an Introduction to Crime Scene Reconstruction* (CRC, Boca Raton, 2008).
[2] D. Attinger, C. Moore, A. Donaldson, A. Jafari, and H. A. Stone, Fluid dynamics topics in bloodstain pattern analysis: Comparative review and research opportunities, Forensic Sci. Int. **231**, 375 (2013).
[3] S. Weidman, Strengthening forensic science in the United States: A path forward, Committee on Identifying the Needs of the Forensic Sciences Community, National Research Council, 2009, http://www.nap.edu/catalog/12589.html.
[4] P. M. Comiskey, A. L. Yarin, S. Kim, and D. Attinger, Prediction of blood back spatter from a gunshot in bloodstain pattern analysis, Phys. Rev. Fluids **1**, 043201 (2016).
[5] S. Siu, J. Pender, F. Springer, F. Tulleners, and W. Ristenpart. Quantitative differentiation of bloodstain patterns resulting from gunshot and blunt force impacts, J. Forensic Sci. (2017), doi:10.1111/1556-4029.13418.
[6] S. Chandrasekhar, *Hydrodynamic and Hydromagnetic Stability* (Dover, New York, 1981).
[7] M. T. Murzabayev and A. L. Yarin. Dynamics of sprinkler jets, Fluid Dyn. **20**, 715 (1985).
[8] I. V. Roisman, L. Araneo, and C. Tropea, Effect of ambient pressure on penetration of a diesel spray, Int. J. Multiphase Flow **33**, 904 (2007).
[9] P. B. S. Lissaman and C. A. Shollenberger, Formation flight of birds, Science **168**, 1003 (1970).
[10] B. T. Cecchetto, Nonlinear Blood Pattern Reconstruction, M.S. thesis, The University of British Columbia, 2010.
[11] C. R. Varney and F. Gittes, Locating the source of projectile fluid droplets, Am. J. Phys. **79**, 838 (2011).
[12] N. Laan, K. G. de Bruin, D. Slenter, J. Wilhelm, M. Jermy, and D. Bonn, Bloodstain pattern analysis: Implementation of a fluid dynamic model for position determination of victims, Sci. Rep. **5**, 11461 (2015).
[13] H. Lamb, *Hydrodynamics* (Cambridge University Press, Cambridge, England, 1959).
[14] N. E. Kochin, I. A. Kibel, and N. V. Rose, *Theoretical Hydrodynamics* (Interscience, New York, 1964).
[15] G. K. Batchelor, *An Introduction to Fluid Dynamics* (Cambridge University Press, Cambridge, England, 2002).
[16] A. L. Yarin, I. V. Roisman, and C. Tropea, *Collision Phenomena in Liquids and Solids* (Cambridge University Press, Cambridge, England, 2017).
[17] G. V. Logvinovich, *Hydrodynamics of Flows with Free Boundaries* (Naukova Dumka, Kiev, 1969) (in Russian).
[18] A. Y. Sagomonyan, *Penetration* (Moscow University Publishing House, Moscow, 1974) (in Russian).
[19] P. M. Comiskey, A. L. Yarin, and D. Attinger, High-speed video analysis of forward and backward spattered blood droplets, Forensic Sci. Int. **276**, 134 (2017).
[20] J. H. McMillen and E. N. Harvey, A spark shadowgraphic study of body waves in water, J. Appl. Phys. **17**, 541 (1946).
[21] J. M. Aristoff and J. W. M. Bush, Water entry of small hydrophobic spheres, J. Fluid Mech. **619**, 45 (2009).
[22] J. H. McMillen, R. L. Kramer, and D. E. Allmand, Impact flash at high speed water entry, J. Appl. Phys. **22**, 360 (1951).
[23] J. H. McMillen, R. L. Kramer, and D. E. Allmand, Shadowgrams of spherical missiles entering water at supersonic speeds, J. Appl. Phys. **21**, 1341 (1950).
[24] A. L. Yarin and D. A. Weiss, Impact of drops on solid surfaces: Self-similar capillary waves, and splashing as a new type of kinematic discontinuity, J. Fluid Mech. **283**, 141 (1995).

[25] A. L. Yarin, Self-similarity, in *Springer Handbook of Experimental Fluid Mechanics*, edited by C. Tropea, A. L. Yarin, and J. F. Foss (Springer, Heidelberg, 2007), pp. 57–82.
[26] G. Birkhoff and R. Isaacs, Transient cavities in air-water entry, Navord Rep.1490 (1951)
[27] A. May, Vertical entry of missiles into water, J. Appl. Phys. **23**, 1362 (1952).
[28] H. Wagner, Über stoß- und gleitvorgänge an der oberfläche von flüssigkeiten. ZAMM **12**, 193 (1932).
[29] S. D. Howison, J. R. Ockendon, and S. K. Wilson, Incompressible water-entry problems at small deadrise angles, J. Fluid Mech. **222**, 215 (1991).
[30] A. A. Korobkin and V. V. Pukhnachov, Initial stage of water impact, Annu. Rev. Fluid Mech. **20**, 159 (1988).
[31] J. O. Marston and S. T. Thoroddsen, Ejecta evolution during cone impact, J. Fluid Mech. **752**, 410 (2014).
[32] B. Karger, R. Nüsse, G. Schroeder, and S. Wüstenbecker, Backspatter from experimental close-range shots to the head, Int. J. Legal Med. **109**, 66 (1996).
[33] B. L. Scheller and D. W. Bousfield, Newtonian drop impact with a solid surface. AIChE J. **41**, 1357 (1995).
[34] A. L. Yarin, Drop impact dynamics: splashing, spreading, receding, bouncing . . . Annu. Rev. Fluid Mech. **38**, 159 (2006).
[35] C. Antonini, A. Amirfazli, and M. Marengo, Drop impact and wettability: From hydrophilic to superhydrophobic surfaces, Phys. Fluids **24**, 102104 (2012).
[36] A. Kolbasov, P. M. Comiskey, R. P. Sahu, S. Sinha-Ray, A. L. Yarin, B. S. Sikarwar, S. Kim, T. Z. Jubery, and D. Attinger, Blood rheology in shear and uniaxial elongation, Rheol. Acta **55**, 901 (2016).
[37] C. Rizer, *Police Mathematics* (Charles C. Thomas, Springfield, 1955).
[38] R. Sahu, S. Sinha-Ray, A. L. Yarin, and B. Pourdeyhimi, Drop impacts on electrospun nanofiber membranes, Soft Matter **8**, 3957 (2012).